MJoSHT
Malaysian Journal of Science, Health & Technology
[mjosht.usim.edu.my]

Article

Harnessing Green Nitrogen-Doped Zinc Oxide for Efficient Methylene Blue Dye Photocatalytic Degradation in Wastewater Treatment

Ummu Humairah Hashim[1], Shahzulaikha Aiman Mohmed[1], Syahida Suhaimi[1], Maisurah Mukhtar[1], Nur Athirah Mohd Taib[1], and Imam Tazi[2]

[1]*Nano Energy Lab (NEL), Department of Applied Physics, Faculty of Science and Technology, Universiti Sains Islam Malaysia, Negeri Sembilan, 71800, Malaysia.*

[2]*Physics Department, Universitas Islam Negeri Maulana Malik Ibrahim Malang, Malang, 65144, Indonesia.*

Correspondence should be addressed to:
Syahida Suhaimi; syahida@usim.edu.my

Article Info
Article history:
Received:11 November 2024
Accepted: 15 January 2025
Published: 19 February 2025

Academic Editor:
Mohd Hafiz Abu Hassan

Malaysian Journal of Science, Health & Technology

MJoSHT2025, Volume 11, Issue No. 1
eISSN: 2601-0003

https://doi.org/10.33102/mjosht.v11i1.474

***Abstract*— Photocatalysis remains a promising solution for water treatment due to its efficiency, sustainability, and ability to degrade a wide range of contaminants. This study explores the green synthesis of zinc oxide (ZnO/GS) doped with varying weight percent of nitrogen (N) as a photocatalyst. ZnO/GS was synthesized via co-precipitation with zinc nitrate hexahydrate and papaya leaf extract in an aqueous solution, which will be further doped using urea as nitrogen doping. Characterization techniques, including FESEM, EDX, FTIR, and XRD, were employed to analyze the morphology, structural characteristics, surface, and pore volumes of nitrogen-doped green synthesized zinc oxide (N-ZnO/GS). The photocatalytic performance of these samples was evaluated through the photodegradation of methylene blue dye under visible light irradiation. The sample with 10wt%, which is 1 g of dopant, exhibited the optimal results, indicating a homogeneous surface and high crystallinity of N-ZnO/GS synthesized via co-precipitation, demonstrating the best photodegradation efficiency in the photocatalysis process. The findings suggest potential applications in environmental remediation through the degradation of organic pollutants, enhancing wastewater treatment efficacy.**

***Keywords*— Photocatalysis; green synthesis; zinc oxide; nitrogen; methylene blue dye.**

I. INTRODUCTION

Water pollution is a complex global environmental issue due to organic pollutants such as dyes, pesticides, pharmaceuticals, and industrial chemicals, including domestic wastewater. These pollutants can have a significant impact on aquatic ecosystems and human health. Water covers approximately 70% of the Earth's surface, and recent projections indicate that water sources are dwindling and will become scarce in the future [1]. Therefore, to address the issue of organic compound-induced water contamination, long-term solutions must be developed. One of the numerous industries that significantly contribute to water pollution is the textile sector, which frequently contains non-biodegradable dyes. Nanotechnology offers scientific advances across a wide range of industries, including healthcare, consumer goods, energy, materials, and manufacturing. To fully utilize the potential of semiconductor nanoparticles as photocatalysts in environmental applications, heterogeneous photocatalytic degradation mechanisms are necessary.

Zinc oxide (ZnO) is an alternative semiconductor used to eliminate dye contaminants in water. ZnO is a semiconductor with a wide bandgap that has drawn much interest due to its capacity to purge water from pigment impurities and harden through photocatalytic breakdown [2]. It is employed in

photocatalysis as a semiconductor to produce electron-hole pairs on its surface. These pairs subsequently participate in redox reactions with adsorbed species, such as organic dyes, which cause their breakdown or mineralization.

In recent years, titanium dioxide (TiO_2) has been extensively studied for the photocatalytic degradation of various strategies to enhance the photocatalytic activity of TiO_2, including surface modification, doping with other elements, and combining TiO_2 with other substances such as metals, metal oxides, and carbon-based compounds [3]. However, TiO_2 has certain drawbacks, including a relatively large bandgap energy that restricts the amount of visible light that can be absorbed and the potential for electron-hole recombination, which can lower the effectiveness of its photocatalytic activity.

Researchers have faced limitations in choosing the appropriate photocatalyst material for a specific pollutant or water treatment application for a long time. Some of the limitations occur during the studies, including the bandgap energy of the photocatalyst, the type of photocatalyst, and the use of metal oxides or doped metal oxides. The bandgap energy of a photocatalyst determines the wavelength of light that it can absorb and, consequently, its capacity to use solar radiation for photocatalytic activity. Materials that can absorb visible light frequently have lower photocatalytic effectiveness than those that can absorb ultraviolet (UV) light, which limits their applicability in a variety of water treatment applications. Furthermore, an ideal photocatalyst is chosen based on its specific application and desired qualities, such as efficiency, stability, and economy. Researchers continue to create new grades with better features to broaden the scope of potential photocatalysts for different industries.

Researchers have discovered new methods and schemes to act as photocatalysts for photocatalytic decomposition. The synthesis of nanomaterials from microbial and plant species used for medical applications is called 'nanoparticle biosynthesis.' This approach is economical, safe, environmentally friendly, and biocompatible. Various organisms, including plants, bacteria, fungi, and algae, are involved in green synthesis. The mass production of impurity-free ZnO doped with nitrogen is possible. By applying a biomimetic approach and reducing the use of expensive and hazardous chemicals, the catalytic activity of nanoparticles was enhanced. Green synthesis is a functional method for obtaining photocatalysts with photocatalytic activity.

Lastly, there are several methods for synthesizing green ZnO, including microwave-assisted methods, hydrothermal, and co-precipitation methods. In this study, the co-precipitation method has been chosen. The co-precipitation approach enables the two-step synthesis of ZnO by first precipitating the metal hydroxide and then heating the oxide to crystallize it. Additionally, it has numerous advantages over other chemical tactics, including low price, minimal strength intake, and capability for large-scale manufacturing [4]. Moreover, these methods are readily adaptable to green synthesis, including the fabrication of TiO_2 and ZnO nanostructures. This study was conducted using the co-precipitation method, which can accelerate pure ZnO and green nitrogen-doped ZnO under light irradiation.

II. MATERIAL AND METHOD

The co-precipitation method was employed to produce N-ZnO/GS. This is generally quite comparable to the preparation of green ZnO nanostructures using the plant extract-mediated co-precipitation method. The plant extracts and precursor solutions were mixed under agitation. Then, by changing the temperature or pH value of the mixture (by adding NaOH), the precipitation process and hydroxide formation are initiated. Third, the precipitate (manually or by centrifugation) was separated, washed with deionized water, and dried at low temperatures. In the final step, high-temperature heat treatment (calcination) was used to crystallize the oxide. The process of the co-precipitation method is simplified in Figure 1.

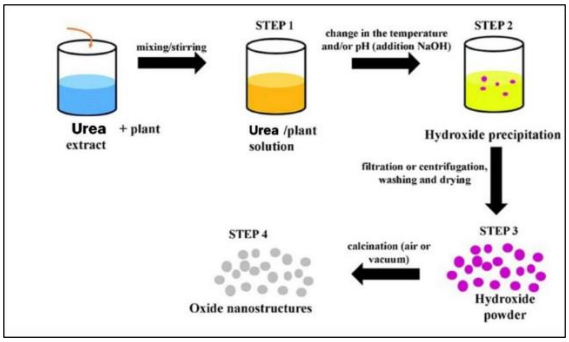

Figure 1. Schematic diagram of co-precipitation method [5].

A. *Preparation of green synthesis of ZnO*

Green synthesis of ZnO was prepared by extracting the extract from *Carica papaya* leaf. The dried leaves were then mixed with deionized water. The sample mixture will then be stirred and heated on a heating mantle for 30 minutes and 60°C, respectively. Subsequently, the mixture was cooled, and the liquid extract was stored in a laboratory freezer.

Figure 2. Schematic diagram of papaya leaves extraction process

B. *Synthesizing of Green Nitrogen-Doped Zinc Oxide*

30 mL of Carica papaya extract was added to a flat-bottom flask containing 0.7 M zinc nitrate hexahydrate [$Zn(NO_3)2.6H_2O$], and the mixture was agitated at 50 rpm for 60 minutes. The pH of the liquid was changed to 12 using an aqueous NaOH solution to ensure that the green zinc oxide particles had fully precipitated and the settling particles weighed a total of 9.8 g.

Subsequently, 30 mL of deionized water and a flask with a flat bottom were filled with 1 g of urea and 9.8 g of green zinc oxide. The mixture was vigorously stirred at 80 rpm for six hours and allowed to stand for 30 minutes. The remaining solid was then oven-dried at 100°C for 6 hours after the liquid layer in the upper region was decanted. In the muffle furnace, the resulting solid material (green zinc oxide doped nitrogen) will be calcined at 350°C for two hours. The procedure will then be performed with urea at various masses ranging from 0.2 g to 2g.

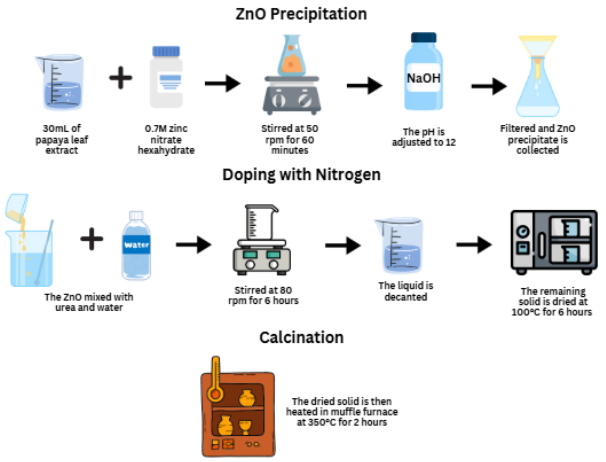

Figure 3. Schematic diagram of the synthesis of N-ZnO/GS

C. *Photocatalysis*

The effectiveness of N-ZnO/GS was assessed in a photocatalytic experiment on the degradation of methylene blue dye compounds in synthetic wastewater. A beaker was filled with 0.1 g of photocatalyst and methylene blue dye solution (100 mL). The heated plate stirrer was switched on, and the solution was agitated in the dark for 15 minutes to reach an equilibrium between adsorption and desorption. An isolated box with a UV lamp was used to produce a dark atmosphere. After 15 minutes, 5 mL of MB was collected and labelled as T_o.

The combination was then exposed to UV light for three hours to determine whether the photocatalytic process took place. The solution was collected every 30 minutes under continuous stirring. The UV light used had a wavelength of 365 nm. All the samples were examined and analyzed using UV-Vis spectroscopy. Figure 4 displays a schematic diagram of the experimental setup for methylene blue dye photodegradation.

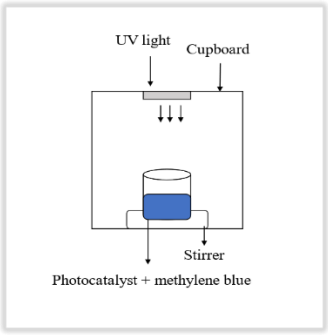

Figure 4. Experimental setup of methylene blue dye photodegradation process

III. RESULTS AND DISCUSSION

Based on this research, various results were obtained using the proposed precipitation method to synthesize N-ZnO/GS nanostructures. The three samples of N-ZnO/GS vary in the different doping masses of urea (carbamide), which are 1.0 g, 1.2 g, and 2.0 g urea. The first four sections discuss the structural properties of N-ZnO/GS using FESEM, EDX, XRD, and FTIR analyses. Then, the photocatalytic reaction and the efficiency of the reaction are explained by UV-Vis spectroscopy.

A. *FESEM*

FESEM provides topographical and elemental information at magnifications ranging from 10 to 300,000 kX, with an almost infinite depth of focus. In this study, all three samples were analyzed at a magnification of 25 kX and 100 kX at 2.00 kV. An illustration of the top view of the nanoflakes generated on the surface by FESEM is displayed in the following figure. Figures 5, 6, and 7 represent 1.0 g, 1.2 g, and 2.0 g of masses doping urea, respectively.

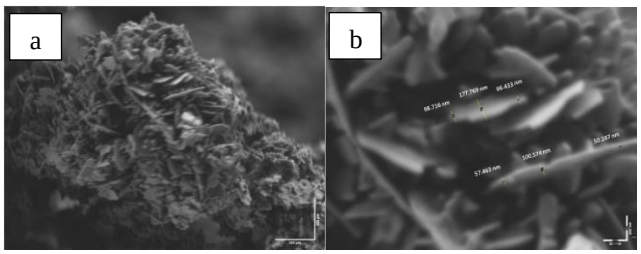

Figure 5. N-ZnO/GS nanoflakes of 1.0 g urea at (a) 25 kx magnification and (b) 100 kx magnification

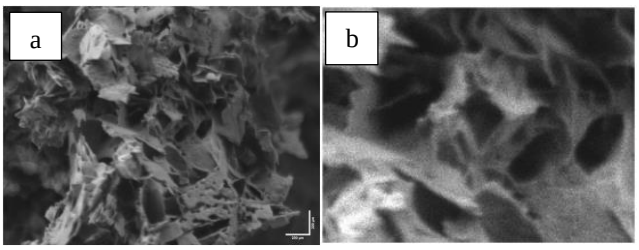

Figure 6. N-ZnO/GS nanoflakes of 1.2 g urea at (a) 25 kx magnification and (b) 100 kx magnification

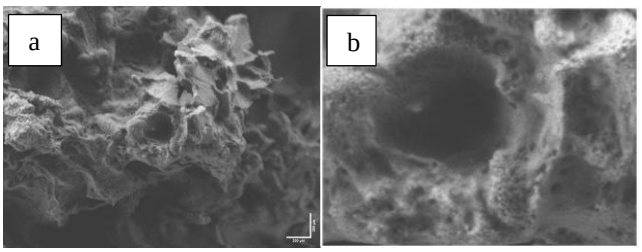

Figure 7. N-ZnO/GS nanoflakes of 2.0 g urea at (d) 25 kx magnification and (f) 100 kx magnification

The morphology of the N-ZnO/GS nanoflakes showed that the green synthesis of N-doped ZnO nanoflakes exhibits a flat, thin, and plate-like nanostructure despite their variation due to the doping masses. Since the morphologies of the three samples differed, it was evident that nitrogen had a significant influence on the structural characteristics. Green synthesis positively impacted the photocatalyst and may have enhanced the overall effectiveness of the photocatalytic process, as indicated by the increased surface area of the green nitrogen-doped ZnO.

In Figures 5(a) and 5(b), the doping mass of urea was the lowest at 1.0 g. It can be clearly observed that the sample consists of nanoflakes that are larger in size than other nanoflakes in the image. The growth of ZnO nanoflake is a facile and cost-effective green technique compared with other chemical synthesis processes [6][7]. For this nitrogen doping method, most of the structures appear as irregular rod-like

particles. Figure 3(b) illustrates that, at a higher magnification of 100 kX, G.S. N-ZnO nanoflakes were discovered to have an average particle size of approximately 975 nm, with particle sizes ranging from 700 nm to 1300 nm. The images suggest that the heating reaction powder had a morphology resembling a network of G.S. N-ZnO flakes. This may be due to the fact that gaseous byproducts are quickly released during the heating reaction [8].

As the doping masses of urea were increased to 1.2 g, the FESEM image in Figure 6(b) depicts that the N-ZnO/GS had a porous structure consisting of flake-shaped particles. Compared with the nanoflakes without pores, the nanoflakes with pores can significantly reduce the volume density with wide absorption bandwidths [9].

In Figure 7(b), the result is similar to Figure 6(b). However, it has bigger pore features compared to Figure 6(b), as the whole substrate surface was covered with high density when the sample was grown at 2.0 g of doping urea. There are indications that the nanoflakes in The FESEM images display that nanoflakes are connected to each other and create a porous structure. This implies that individual nanoflakes are part of a larger, more interconnected structure than isolated objects. The composite has a particularly high specific surface area, as well as pore characteristics, which results in enhanced photocatalyst performance [10].

B. EDX

The purity and elemental composition of the samples were determined using energy-dispersive X-ray spectroscopy (EDX). Figure 4.4 displays the EDX analysis recorded at three different doping masses of urea (carbamide), which are 1.0 g, 1.2 g, and 2.0 g of urea. This analysis was performed to identify the components of N-ZnO/GS. Zinc, followed by oxygen, was the most abundant element in the nanostructure in all samples, as displayed in the spectra in Figure 8. Carbon (C) was present in the spectra of all samples, which might be a consequence of heating. Silicon (Si) is probably present since ZnO is produced on a silicon substrate. Calcium (Ca) and Aluminium (Al) might have originated from the substrate and holder material, respectively. However, compared to the other components present in all three samples, Zn and O were reported to dominate the proportion of materials, indicating that the acquired N-ZnO/GS sample is of good quality.

Elemental mapping is displayed in Figure 9 for each of the three samples with varying doping masses of urea. This indicates that the components are dispersed evenly rather than concentrated in one area, as portrayed in Figures 9(a) and 9(b), indicating that the N-ZnO/GS nanoflakes in each sample are well-grown. However, in Figure 9(c), a 2.0 g doping mass of urea does not demonstrate good dispersion in the oxygen and carbon area due to uneven distribution or aggregation of the elements when preparing the sample.

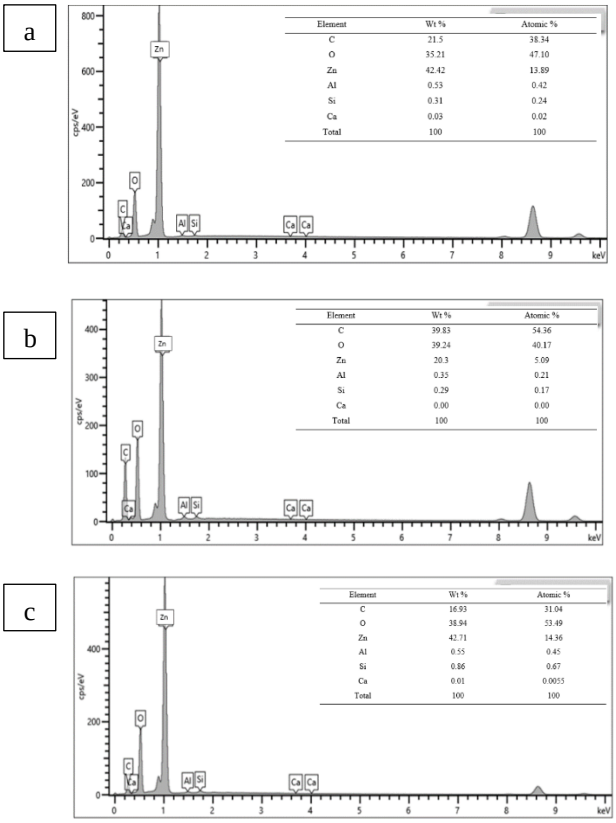

Figure 8. EDX spectra with different doping ratios of urea (a) 1.0 g of urea, (b) 1.2 g of urea, and (c) 2.0 g of urea

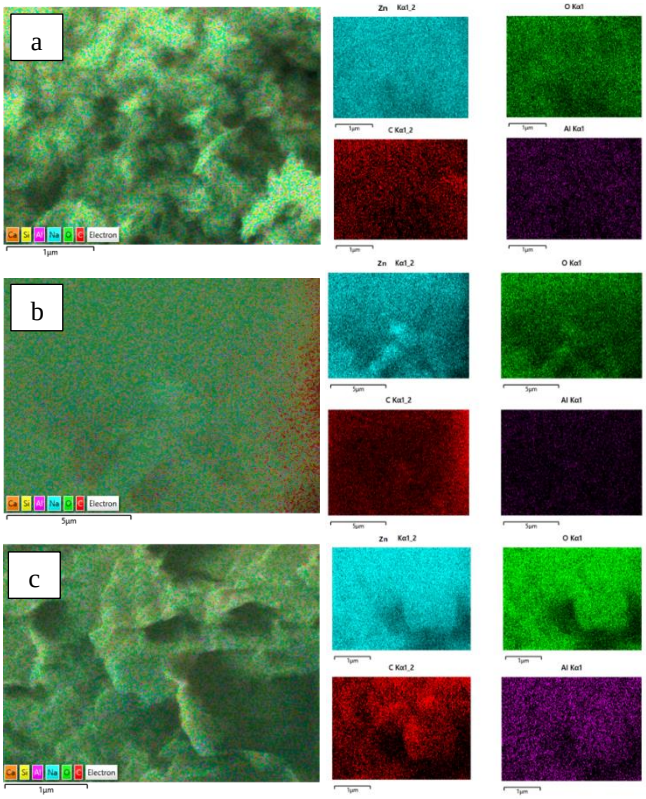

Figure 9. The overall and elemental EDX mapping of N-ZnO/GS with different doping ratios (a) 1.0 g of urea, (b) 1.2 g of urea, and (c) 2.0 g of urea

C. FTIR

FTIR spectroscopy was employed to examine the functional groups of the N-ZnO/GS. The wave number range of 4000 – 500 cm^{-1} reveals the functional groupings. As displayed in Figure 10, the urea masses in the spectra of the green synthesis of nitrogen-doped zinc oxide demonstrated four distinct peaks. The peaks are clearly indicated together with the groups and classes in Table I.

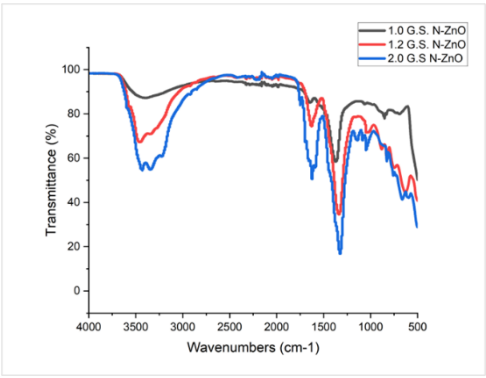

Figure 10. FTIR Spectra for N-ZnO/GS with different doping ratios of urea (a) 1.0 g of urea, (b) 1.2 g of urea, (c) 2.0 g of urea, and (d) pure ZnO

TABLE I. FREQUENCY TABLE

	Peaks (cm^{-1})	Group	Class
Sample 1	3394.69	N-H stretching	Aliphatic primary amine
	1643.47	C=C stretching	Conjugated alkene
	1372.56	O-H bending	Phenol
	688.04	C=C bending	Alkene
Sample 2	3452.65	O-H stretching	Alcohol
	1626.66	C=C stretching	Alkene
	1336.98	C-N stretching	Aromatic amine
	882.05	C-H bending	1,3-disubstituted
Sample 3	3346.16	N-H stretching	Secondary amine
	1588.86	N-H bending	Amine
	1324.96	C-N stretching	Aromatic amine
	827.42	C=C bending	Alkene

As indicated in Figure 10, four peaks were present in the 1.0 g, 1.2 g, and 2.0 g doping masses of urea. The peaks and their corresponding groups and classes are presented in Table I for sample 1. The third peak (3394.69 cm^{-1}) is attributed to N-H stretching, confirming the presence of nitrogen arising from doping on the photocatalyst. However, the research by Prabakaran et al. stated that N-O stretching was present within the magnificence of the 1000-1200 cm^{-1} peak in the FTIR spectra [11]. Hence, considering that H prefers to interact with N at the anti-bonding site and form an N–H complex, this peak clearly demonstrates the passivation of N-ZnO by H [12]. This result confirms that N replaces O in the ZnO lattice.

For sample 2, a peak at 3452.65 cm^{-1} is observed and could be associated with the stretching modes of the hydroxyl group (O-H). Carbon and nitrogen in nitrogen-doped ZnO film have previously been reported to have some associations [13]. In addition, the nitrogen dopant arises from the FTIR spectra, which gives the value of wavenumber (1136.98 cm^{-1}), which belongs to C-N stretching. Extremely strong infrared absorption peaks for the nitrogen-doped ZnO films were observed in the frequency range, corresponding to the N–C, N–N, and C–O modes. For Sample 3, there are three peaks presented in the figure above that indicate the presence of nitrogen as it has a higher doping mass of urea than the other samples.

D. XRD

XRD analysis was conducted to confirm the crystal structure of the N-ZnO/GS. Figure 11 displays the representative XRD patterns, which exhibit a few sharp peaks attributed to the high-purity phases of the N-ZnO/GS nanostructures. All samples varied according to the amount of urea, as mentioned previously. Samples 1, 2, and 3 possess 1.0 g, 1.2 g, and 2.0 g masses of urea, respectively. The highest peak for each sample was recorded, which has (101) orientation on the plane with a mean angle of $2\theta \approx 36.22°$. The hexagonal wurtzite structure of ZnO is well supported by the diffraction peaks [14]. Since the synthesized ZnO was highly oriented, the c-axis must have grown perpendicular to the substrate surface, as indicated by the steep peak in the (101) plane [15]. While Sample 3 has a low peak, which denotes low crystallinity, and its utilization of 2.0 g of doping urea are opposites in terms of each other. The crystallinity of the N-ZnO/GS, which involves the nucleation and growth mechanism, is thus affected by the doping masses of urea, as can be seen.

The XRD results were examined to determine the average crystallite size of the N-ZnO/GS nanostructures. The crystal size (D) of the films was estimated using Scherrer's equation and the plane of the zincite phase.

$$D = \frac{0.89\,\lambda}{ß\cos\theta}, \quad (1)$$

where D is the photocatalyst's crystallite size, 0.154056 nm is the wavelength of the X-ray beam, ß is full width at half maximum, and Θ is the angle of diffraction. According to Table II, the average crystallite sizes of samples one, two, and three were 28.52 nm, 29.27 nm, and 13.80 nm, respectively. The pure ZnO sample, sample four, has an average value of 46.76 nm, which is greater than the other values. The value of D exhibited an increment when the urea doping masses climbed from 1.0 g to 1.2 g and an inclination when the urea doping masses increased to 2.0 g. This is due to the increase in the pore features on the surface of Sample 2. Nevertheless, the crystallite size decreased at 2.0 g, possibly due to an alternative concentration-dependent impact.

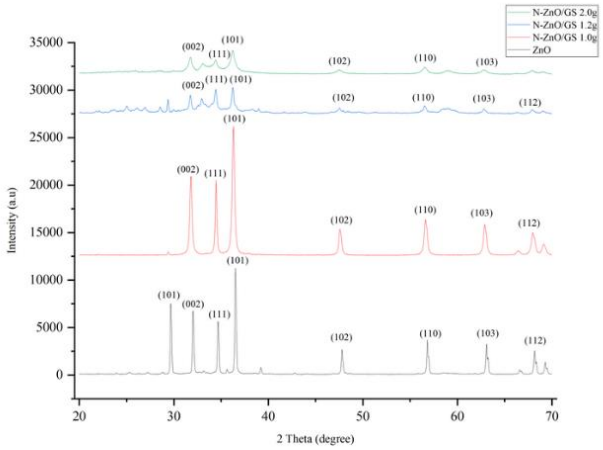

Figure 11. XRD spectra for N-ZnO/GS with different doping ratios of urea (a) 1.0 g of urea, (b) 1.2 g of urea, (c) 2.0 g of urea, and (d) pure ZnO

TABLE II. MEASUREMENT AND STRUCTURAL CALCULATION OF N-ZNO/GS NANOSTRUCTURES

Sample	Dopant (g)	hkl plane	Lattice spacing, d	2θ (°)	Crystallite size, D (nm)
S1	1.0	(101)	2.475	36.26	28.52
S2	1.2	(101)	2.475	36.24	29.27
S3	2.0	(101)	2.475	36.24	13.80
S4	-	(101)	2.478	36.52	46.76

Table III provides a comparison of ZnO from the JCPDS library. From the table, it is clear that all three samples are similar to ZnO from the JCPDS library. Thus, it can be concluded that the synthesized ZnO has a good characteristic for the crystallographic part.

TABLE III. THE XRD CRYSTALLOGRAPHIC DATA AND LATTICE PARAMETER OF JCPDS AND VARIED DOPING MASSES OF UREA

Sample	a (Å)	c (Å)	Volume (Å)	c/a
ZnO JCPDS	3.2490	5.2050	47.583	1.602
S1	3.2494	5.2054	47.598	1.602
S2	3.2494	5.2054	47.598	1.602
S3	3.2494	5.2054	47.598	1.602
S4	3.2533	5.2073	47.730	1.601

E. Photocatalysis

UV-Vis spectroscopy refers to the absorption or reflectance of molecules in the ultraviolet-visible region using light from the visible and adjacent ranges. The experiment began with the measurement of 5 mL (T_0) of the methylene blue dye. 5 mL of the methylene blue dye was added every 30 minutes until the 180-minute mark was reached. Assigned the numbers T_1, T_2, T_3, T_4, T_5, and T_6 correspond to the solutions obtained after 30, 60, 90, 120, 150, and 180 minutes, respectively.

The time-dependent absorption spectra of the MB aqueous solutions in the presence of N-ZnO/GS upon exposure to visible light are displayed in Figure 12. The peak at 662 nm, which is the highest of the three samples and can be seen in the image, was subsequently selected to track the photocatalytic degradation process.

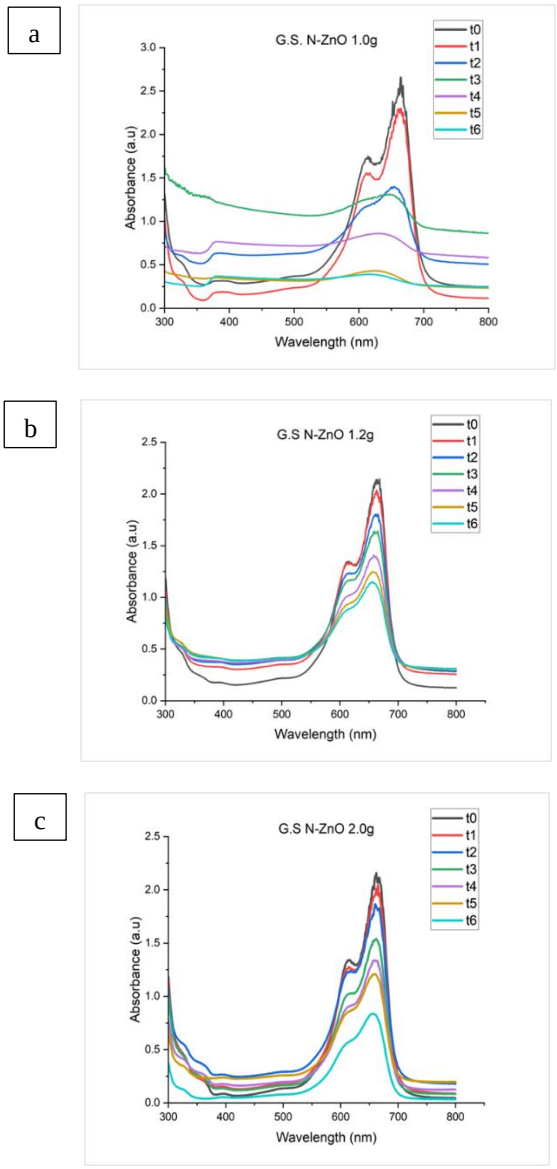

Figure 12. UV-Vis spectra of N-ZnO/GS with (a) 1.0 g, (b) 1.2 g, and (c) 2.0 g doping masses of urea

Equation 2 can be used to determine the efficiency of photocatalytic activity. The percentage of photodegradation and the percentage removal of MB dye of N-ZnO/GS are summarized in Tables IV, V, and VI for each sample. The percentage removal of MB dye was calculated using Equation 3.

$$D\% = \frac{Ao-A}{Ao} \times 100. \quad (2)$$

$$Percentage\ removal\ (\%) = \frac{Co-Ct}{Co} \times 100. \quad (3)$$

A graph based on Table IV is displayed in Figure 13. A trend of increasing photodegradation percentage can be clearly seen in the figure for all three samples. The photodegradation percentage of the first sample increased to 84.77% over time. The green nitrogen-doped ZnO nanostructure that was

synthesized and doped with 1.0 g of urea is an excellent photocatalyst with good performance, as demonstrated in the figure. Next, for the sample with a 1.2 g doping mass of urea in N-ZnO/GS (which is sample 2), the photodegradation percentage increased to 46.02%, indicating a slight deterioration in photodegradation efficiency over time. Subsequently, as the reaction progressed, the photodegradation percentage in Figure 13 for sample 3 increased linearly to 60.60%. This sample, which contains a 2.0 g doping mass of urea, performs better as a photocatalyst than the 1.2 g doping mass of urea.

TABLE IV. PHOTODEGRADATION PERCENTAGE PROCESS OVER TIME FOR N-ZNO/GS AS PHOTOCATALYST

Sample collected by time	Time (minutes)	Photodegradation Percentage (%)		
		S1	S2	S3
T0	15	0.00	0.00	0.00
T1	30	13.23	5.49	5.79
T2	60	46.88	15.43	12.91
T3	90	50.56	23.00	28.97
T4	120	67.34	33.98	37.87
T5	150	83.24	41.19	44.11
T6	180	84.77	46.02	60.60

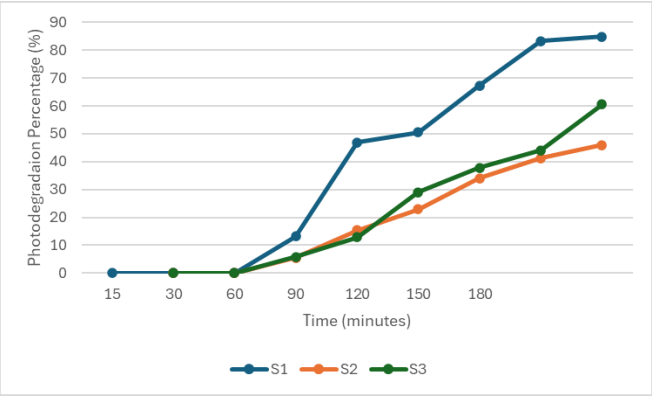

Figure 13. The photodegradation percentage process over time graph for various N-ZnO/GS as photocatalyst

The percentage of methylene blue dye removed was also determined. As time increased, the trend of the graph in Figure 14 illustrates a pattern that indicates a reduction in the percentage removal of methylene blue dye. After 30 minutes of photocatalyst with 1.0 g of urea dopant exposed to UV light, the proportion of methylene blue dye started at 86.79%. At the end of the process, only 15.23% of the methylene blue dye remained. There was a noticeable pattern as the initial percentage of 94.51% dropped to 53.98% for Sample 2. Finally, the proportion of methylene blue dye at the start of the experiment for sample 3, which possesses 2.0 g of urea, was 94.21% when the photocatalyst was exposed to UV light for the first half hour. After 180 minutes, it steadily decreased until it reached 39.40% methylene blue dye.

TABLE V. REMOVAL PERCENTAGE OF METHYLENE BLUE OVER TIME FOR N-ZNO/GS AS PHOTOCATALYST

Sample collected by time	Time (minutes)	Removal Percentage (%)		
		S1	S2	S3
T0	15	0.00	0.00	0.00
T1	30	86.79	94.51	94.21
T2	60	53.12	84.56	87.09
T3	90	49.44	76.99	71.03
T4	120	32.66	66.02	62.13
T5	150	16.76	58.81	55.88
T6	180	15.23	53.98	39.40

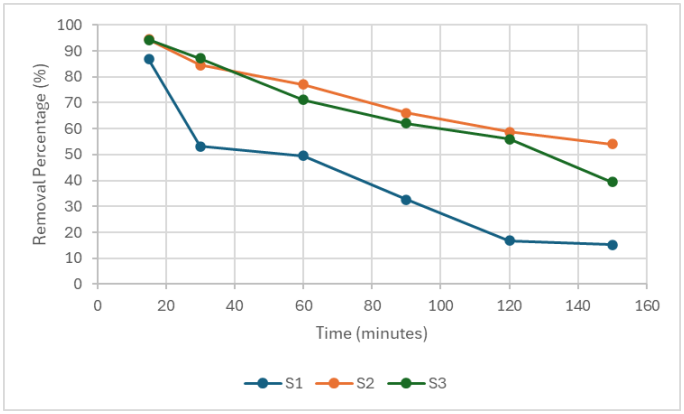

Figure 14. The removal percentage of methylene blue over time graph for various N-ZnO/GS as photocatalyst

IV. CONCLUSIONS

This research has investigated the three distinct doping masses of urea (1.0 g, 1.2 g, and 2.0 g) in green synthesized nitrogen-doped zinc oxide (N-ZnO/GS) using zinc nitrate hexahydrate, urea, and liquid extract from papaya plants. With the use of FESEM-EDX, FTIR, and XRD analysis, the morphology, functional groups, surface characteristics, and crystallinity of 1.0 g, 1.2 g, and 2.0 g doping mass of urea in N-ZnO/GS were investigated. Doping and green synthesis were effectively carried out during the photocatalyst preparation stage, as evidenced by the noticeable differences in the findings from the FESEM-EDX, FTIR, and XRD examinations for the 1.0 g, 1.2 g, and 2.0 g doping masses of urea in N-ZnO/GS. The ideal MB degradation percentages in N-ZnO/GS were 84.77%, 46.02%, and 60.60% for urea doping masses of 1.0, 1.2, and 2.0 g, respectively.

In summary, the limited scope indicates that 1.0 g of urea is the most optimal doping mass for synthesizing N-ZnO/GS. The study's findings revealed that green synthesis and less doping significantly improved the capacity of ZnO for photocatalysis, which in turn increased the breakdown of MB dye. This research demonstrated the economic viability of wastewater treatment through the degradation of organic pollutants under sunlight exposure, suggesting the potential applicability of this method in extensive wastewater treatment infrastructures.

FUTURE PERSPECTIVES

Photocatalytic processes are acknowledged as promising technologies that can safely and cleanly solve energy and environmental issues without the need for additional energy-intensive equipment. The practical use of photocatalysis on an industrial scale is still relatively restricted, although much research has been conducted on photocatalysts. In-depth efforts are required to overcome diverse barriers and enhance the viability of this generation in the future. First, a significant advancement in photocatalysis is the use of sunlight as a light source, which holds promise for improving the overall effectiveness and usefulness of the technology. Through the strategic integration of sunlight, the photocatalytic process can utilize a wider range of wavelengths from the solar spectrum, including both UV and visible light. Changing from the traditional method of depending only on UV light takes care of a significant technological shortcoming that has limited penetration into complex environmental matrices. The wide range of wavelengths emitted by sunlight guarantees a complete activation of the green zinc oxide-doped nitrogen photocatalyst, creating opportunities for a more potent and adaptable reaction to various environmental factors and water contaminants.

Furthermore, the synthesis of nanostructures may lead to additional traits. Photocatalysis frequently improves the performance of photocatalytic processes. Notwithstanding the reality that present techniques might also yield terrific photocatalysts with large surface vicinity, tiny particle length, extended fee service lifetime, and different traits, further research is required in this region. Additionally, it is necessary to address operational concerns, such as the photoactivity of recycled photocatalysts and photocatalyst loss and recovery throughout the submit-remedy. To predict the quantum yield, kinetics, and perfect technique parameters for photocatalytic structures used in water remedies, more thorough research is essential to develop and evaluate mathematical models [16].

The promise of this technology, particularly in the realm of environmental applications such as photocatalytic degradation of pollutants, necessitates meticulous exploration of methods to scale up production. The process of scaling up entails modifying current laboratory procedures to handle greater numbers and volumes while preserving efficacy and economy. Understanding the practical and economic aspects of industrial-scale production is crucial. The availability of raw materials, potential financial consequences, energy use, and overall process efficiency are key factors in assessing whether a large-scale implementation is feasible. The research should focus on improving the synthesis techniques to guarantee repeatable and consistent results on a larger scale. Moreover, it is also critical to look into economical and sustainable raw material sources, such as Carica papaya leaf extract, and determine how much energy will be needed for operations that are expanded [17].

Green zinc oxide doped nitrogen production has great potential, and addressing its scalability will help make it an industrially feasible alternative for large-scale environmental cleanup projects. Making environmentally friendly solutions practical and impactful for everyday use is the ultimate aim, and the path towards scalable procedures aligns with this objective.

CONFLICT OF INTEREST

I hereby declare that the disclosed information is correct and that there are no conflicts of interest with the other authors.

ACKNOWLEDGEMENT

This work was supported by the Universiti Sains Islam Malaysia [PPPI/FST/0121/USIM/15521] and the Faculty of Science & Technology located at USIM by providing a laboratory with sufficient facilities throughout the experimental work.

REFERENCES

[1] W. Tang, B.D. Chen, and Z. L. Wang, "Recent Progress in Power Generation from Water/Liquid Droplet Interaction with Solid Surfaces," *Advanced Functional Materials*, vol. 29, no. 41, Mar. 2019, doi: https://doi.org/10.1002/adfm.201901069

[2] B. H. Alshammari, M. M. Lashin, M. A. Mahmood, F. S. Al-Mubaddel, N. Ilyas, N. Rahman, M. Sohail, A. Khan, S. S. Abdullaev and R. Khan, "Organic and inorganic nanomaterials: fabrication, properties and applications," RSC Advances, vol. 13, no. 20, pp. 13735–13785, May 2023, doi: https://doi.org/10.1039/d3ra01421e

[3] J. Musial, D. T. Mlynarczyk, and B. J. Stanisz, "Photocatalytic degradation of sulfamethoxazole using TiO -based materials – Perspectives for the development of a sustainable water treatment technology," *The Science of The Total Environment*, vol. 856, pp. 159122–159122, Jan. 2023, doi: https://doi.org/10.1016/j.eti.2024.103763

[4] R. Jeyachitra, S. Kalpana, T. S. Senthil, and M. Kang, "Electrical behavior and enhanced photocatalytic activity of (Ag, Ni) co-doped ZnO nanoparticles synthesized from co-precipitation technique," *Water Science and Technology*, vol. 81, no. 6, pp. 1296–1307, Mar. 2020, doi: https://doi.org/10.2166/wst.2020.230

[5] R. A. Gonçalves, R. P. Toledo, N. Joshi, and O. M. Berengue, "Green Synthesis and Applications of ZnO and TiO_2 Nanostructures," *Molecules*, vol. 26, no. 8, pp. 2236–2236, Apr. 2021, doi: https://doi.org/10.3390/molecules26082236

[6] F. Quddus, A. Shah, Faiza Jan Iftikhar, Noor Samad Shah, and A. Haleem, "Environmentally Benign Nanoparticles for the Photocatalytic Degradation of Pharmaceutical Drugs," *Catalysts*, vol. 13, no. 3, pp. 511–511, Mar. 2023, doi: https://doi.org/10.3390/catal13030511

[7] S. A. Patil, Pallavi Bhaktapralhad Jagdale, A. Singh, R. V. Singh, Z. Khan, Akshaya Kumar Samal, and M. Saxena, "2D Zinc Oxide – Synthesis, Methodologies, Reaction Mechanism, and Applications," Small, vol. 19, no. 14, Jan. 2023, doi: https://doi.org/10.1002/smll.202206063

[8] S. C. Singh, "Zinc oxide nanostructures: Synthesis, characterizations and device applications". Journal of Nanoengineering and Nanomanufacturing, vol 3(4), pp. 283-310, 2013, doi: 10.1166/jnan.2013.1147

[9] T. Kuan, and H. Man-Gui, "Micromagnetics simulation on the microwave permeability of magnetic porous nanoflakes," *Dntb.gov.ua*, 2015, doi: 10.7498/aps.64.237501

[10] C. Chen, M. Li, K. Shen, L. Yang, and Z. Chen, "Structural design and antibacterial properties of porous SiO_2 /ZnO /Cu_2O composites," *Research Square (Research Square)*, Feb. 2023, https://doi.org/10.1166/mex.2024.2631

[11] E. Prabakaran and K. Pillay, "Synthesis of N-doped ZnO nanoparticles with cabbage morphology as a catalyst for the efficient photocatalytic degradation of methylene blue under UV and visible light," *RSC Advances*, vol. 9, no. 13, pp. 7509–7535, Jan. 2019, doi: 10.1039/C8RA09962F

[12] S. Limpijumnong, X. Li, S.-H. Wei, and S. B. Zhang, "Probing deactivations in Nitrogen doped ZnO by vibrational signatures: A first principles study," *Physica B Condensed Matter*, vol. 376–377, pp. 686–689, Jan. 2006, doi: https://doi.org/10.1016/j.physb.2005.12.172.

[13] T. Li, Y. Zhu, X. Ji, W. Zheng, Z. Lin, X. Lu, and F. Huang, "Experimental Evidence on Stability of N Substitution for O in ZnO Lattice," *The Journal of Physical Chemistry Letters*, Oct. 06, 2020, https://doi.org/10.1021/acs.jpclett.0c02698

[14] T. Ahmad, V. Pandey, M. Saddam Husain, Adiba, and S. Munjal, "Structural and spectroscopic analysis of pure phase hexagonal wurtzite ZnO nanoparticles synthesized by sol-gel," *Materials Today:*

Proceedings, vol. 49, pp. 1694–1697, 2022, https://doi.org/10.1016/j.matpr.2021.07.456

[15] P. Gu, X. Zhu, and D. Yang, "Vertically aligned ZnO nanorods arrays grown by chemical bath deposition for ultraviolet photodetectors with high response performance," *Journal of Alloys and Compounds*, vol. 815, pp. 152346–152346, Sep. 2019, doi: https://doi.org/10.1016/j.jallcom.2019.152346.

[16] B. Samanta, Ángel Morales-García, F. Illas, N. Goga, J. A. Anta, S. Calero, A. Bieberle-Hütter, Florian Libisch, A. B. Muñoz-García, M. Pavone, and Maytal Caspary Toroker, "Challenges of modeling nanostructured materials for photocatalytic water splitting," Chemical Society Reviews, vol. 51, no. 9, pp. 3794–3818, 2022, doi: https://doi.org/10.1039/d1cs00648g.

[17] O. Adeyi, E. O. Oke, B. I. Okolo, A. J. Adeyi, J. A. Otolorin, K. Nwosu-Obieogu, J. A. Adeyanju, G. W. Dzarma, S. Okhale, D. Ogu and P. N. Onu, "Process optimization, scale-up studies, economic analysis and risk assessment of phenolic rich bioactive extracts production from Carica papaya L. leaves via heat-assisted extraction technology," *Heliyon*, vol. 8, no. 4, pp. e09216–e09216, Mar. 2022, doi: https://doi.org/10.1016/j.heliyon.2022.e09216.